Available online at www.sciencedirect.com
ScienceDirect
Fluid Phase Equilibria 252 (2007) 57–65
FLUID PHASE EQUILIBRIA
www.elsevier.com/locate/fluid

Generalized crossover description of the thermodynamic and transport properties in pure fluids II. Revision and modifications

S.B. Kiselev *, J.F. Ely

Chemical Engineering Department, Colorado School of Mines, Golden, CO 80401-1887, USA

Received 30 June 2006; received in revised form 25 September 2006; accepted 15 October 2006
Available online 14 December 2006

Abstract

In our previous work [S.B. Kiselev, J.F. Ely, Fluid Phase. Equilib. 222–223 (2004) 149], we developed a generalized cubic (GC) EoS for pure fluids, which incorporates non-analytic scaling laws in the critical region and reproduces the thermodynamic properties of pure fluids with high accuracy, including the asymptotic scaling behavior of the isochoric heat capacity in the one- and two-phase regions. However, it appears that in some cases the GC EoS can give unphysical behavior when extrapolated to high temperatures and densities. In this work, we present a modification of the generalized cubic EoS, which in the critical region is physically equivalent to the GC EoS developed earlier, but is more reliable in its extrapolation to high temperatures.

Keywords: Critical region; Crossover theory; Equation of state; Heat capacity; Thermal conductivity; Carbon dioxide; Ethane; Methane; Water

1. Introduction

It is well known that long-range fluctuations in the density cause the thermodynamic surface of fluids to exhibit a singularity at the critical point. As a consequence, all analytical, classical equations of state (EoS), which give a reasonable representation of the thermodynamic properties of fluids far away from the critical point, fail in the critical region. Significant efforts have been made to develop a "global" EoS that incorporates the asymptotic singular behavior of the thermodynamic properties in the critical region, and at low densities reproduces the ideal gas equation [1–27]. Thus far, all these efforts have been mainly focused on developing an EoS for VLE and PVT surfaces, but not for caloric properties, such as the isochoric and isobaric heat capacities. In our recent publication [28], we reported a "global", generalized cubic (GC) EoS for pure fluids, which reproduces the thermodynamic properties of pure fluids with high accuracy, including the asymptotic scaling behavior of the isochoric heat capacity in the one- and two-phase regions. In combination with the decoupled-mode theory (DMT), we also proposed a generalized GC + DMT model [28] that is capable of reproducing the singular behavior of the thermal conductivity of pure fluids in and beyond the critical region. However, it appears, that for some substances the GC EoS with system-dependent parameters optimized to experimental data at near critical and sub-critical temperatures, can give unphysical behavior at higher temperatures and densities. As an example, the short-dashed curve in Fig. 1 shows the pressure as a function of density calculated with the GC EoS for CO_2 [28] along the isotherm $T = 2T_c$. As one can see, at high densities where $\rho > 1.5\rho_c$, this isotherm CO_2 exhibits non-monotonic behavior, and when $1.5 < \rho/\rho_c < 1.8_c$ it even has a negative slope, $(\partial P/\partial\rho)_T < 0$, which is physically incorrect. We need to note, that this non-monotonic behavior is observed at temperatures which are far beyond the temperature range of the experimental data used for the optimization of the GC EoS for CO_2 [28], and, therefore, was overlooked in our previous work.

In principle, the non-monotonic behavior observed in Fig. 1 can be eliminated by refitting the GC EoS using experimental high temperature PVT-data. Alternatively, one could generate data for $T \geq T_c$ with some more accurate EoS, such as a multi-parameter crossover EoS developed recently for CO_2 by Sun et al. [29]. However, in general these approaches make the GC EoS

* Corresponding author. Tel.: +1 303 273 3190; fax: +1 303 273 3730.
E-mail address: skiselev@mines.edu (S.B. Kiselev).

0378-3812/$ – see front matter © 2006 Elsevier B.V. All rights reserved.
doi:10.1016/j.fluid.2006.10.028

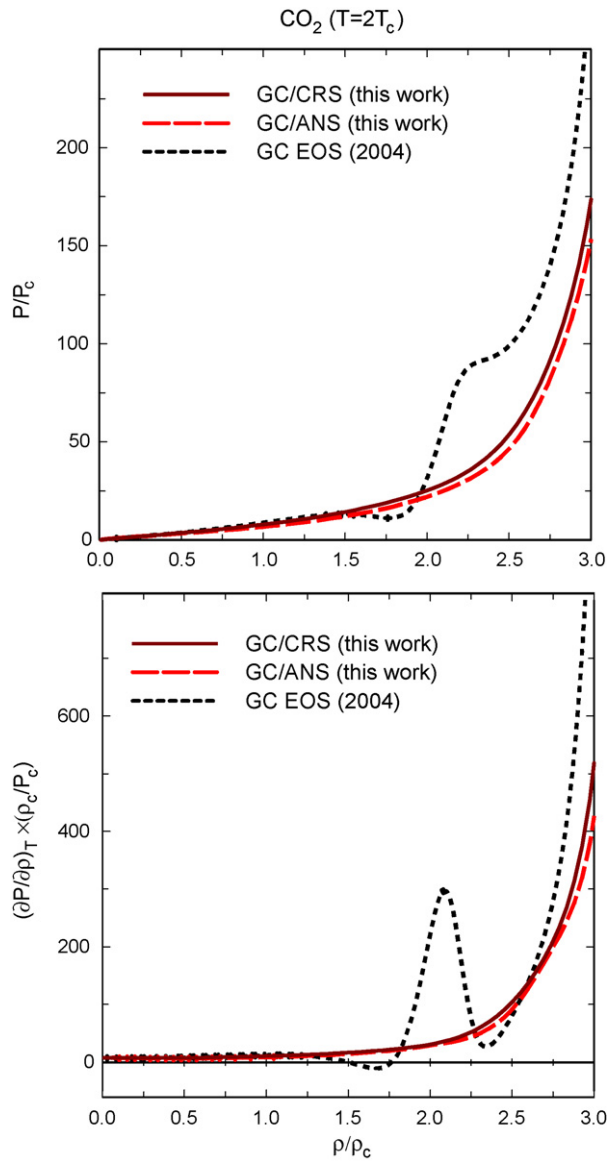

Fig. 1. P–ρ (top) and $(\partial P/\partial\rho)_T - \rho$ (bottom) isotherms calculated for carbon dioxide at $T = 2T_c$ with the GC EoS [28] (short-dashed curves), the GC/CRS (solid curves), and the GC/ANS (long-dashed curves) models.

less predictive. Therefore, in this paper we present a modification of the GC EoS, which is more reliable when extrapolated to high temperatures. We proceed as follows. In Section 2 we describe an improved GC EoS for pure fluids and in Section 3 we apply this EoS for the thermodynamic transport properties calculations.

2. Modified GC EoS

In the generalized—"global" crossover EoS, the dimensionless Helmholtz free energy $\bar{A} = A(T, v)/RT$ is represented in the form [28]:

$$\bar{A}(T, v) = \Delta\bar{A}(\bar{\tau}, \bar{\varphi}) - K(\tau, \varphi) - \Delta v\bar{P}_0(T) + \bar{A}_0^{\mathrm{res}}(T) + \bar{A}_{\mathrm{id}}(T), \quad (1)$$

where $v = 1/\rho$ is molar volume, R the universal gas constant, T_{0c} and v_{0c} are the classical (predicted by the unmodified EoS) critical temperature and molar volume, respectively, $\Delta v_c = (v_c - v_{0c})/v_{0c} \ll 1$ a dimensionless shift of the critical volume, $\bar{P}_0(T) = P(T, v_{0c})/RT$ the dimensionless pressure, $\bar{A}_0^{\mathrm{res}}(T) = \bar{A}^{\mathrm{res}}(T, v_{0c})$ the dimensionless residual part of the Helmholtz energy along the critical isochore $v = v_{0c}$, and $\bar{A}^{\mathrm{id}}(T)$ is the dimensionless temperature-dependent ideal-gas Helmholtz free energy. The singular part of the Helmholtz free energy $\Delta\bar{A}(\bar{\tau}, \bar{\varphi})$ is obtained by a replacing the dimensionless distances $\Delta T = T/T_{0c} - 1$ and $\Delta v = v/v_{0c} - 1$ in the classical expression for critical part of the Helmholtz free energy:

$$\Delta\bar{A}(\Delta T, \Delta v) = \bar{A}^{\mathrm{res}}(\Delta T, \Delta v) - \bar{A}^{\mathrm{res}}(\Delta T, 0) - \ln(\Delta v + 1) + \Delta v\bar{P}_0(\Delta T) \quad (2)$$

with the renormalized values

$$\bar{\tau} = \tau\Upsilon^{-\alpha/2\Delta_1}, \quad \bar{\varphi} = \varphi\Upsilon^{(\gamma-2\beta)/4\Delta_1} + (1+\varphi)\Delta v_c\Upsilon^{(2-\alpha)/2\Delta_1}, \quad (3)$$

where $\alpha = 0.11$, $\beta = 0.325$, $\gamma = 2 - 2\beta - \alpha = 1.24$, and $\Delta_1 = 0.51$ are universal non-classical critical exponents [30,31] v_c, and $\Upsilon(\tau, \varphi)$ denotes a crossover function. In Eqs. (1)–(3), $\tau = T/T_c - 1$ is a dimensionless deviation of the temperature from the real critical temperature T_c, $\varphi = v/v_c - 1$ is a dimensionless deviation of the molar volume form the real critical molar volume, and the kernel term is given by

$$K(\tau, \varphi) = \frac{1}{2}a_{20}\tau^2[\Upsilon^{-\alpha/\Delta_1}(\tau, \varphi) - 1] + \frac{1}{2}a_{21}\tau^2[\Upsilon^{-(\alpha-\Delta_1)/\Delta_1}(\tau, \varphi) - 1], \quad (4)$$

where the coefficients a_{20} and a_{21} correspond to the asymptotic and first Wegner-correction terms, respectively.

In our previous work [28], for the crossover function $\Upsilon(\tau, \eta)$ we used a simple phenomenological expression obtained by Kiselev and co-workers [32–36]:

$$\Upsilon(q) = \left(\frac{q}{1+q}\right)^{2\Delta_1}, \quad (5)$$

where $q = (r/Gi)^{1/2}$ is a renormalized distance to the critical point and $r(\tau, \varphi)$ is a parametric variable. The crossover function Υ given by Eq. (5) coincides with the corresponding crossover function in the asymptotic crossover Leung–Griffiths model obtained in the first order of ε-expansion by Belyakov et al. [37] and works well in the extended critical region where $|\tau| < 1$. However, as was shown by Kiselev et al. [38], better extrapolation behavior of the crossover equation of state to the high temperature region can be achieved with a crossover function obtained in the form of a Pade-approximant to the numerical solution of the renormalization-group equations [39,40]. Therefore, in order to avoid the non-monotonic unphysical behavior of the pressure–density isotherms in the extrapolation of the GC EoS in the high temperature region, we first replace the crossover function Υ in Eq. (3) with the more reliable crossover function

Y obtained by Kiselev et al. [39,40]:

$$Y(\hat{q}) = \left[\frac{\hat{q}+\hat{q}^2}{1+\hat{q}+\hat{q}^2}\right]^{\Delta_1}, \quad (6)$$

where $\hat{q} = r/Gi$. Unlike the original work that incorporated this function [39,40], the parametric variable $r(\tau, \varphi)$ in Eq. (6) can be found from a solution of the crossover sine (CRS) model [38]:

$$\frac{(r-\tau)}{\mathrm{Gi}}\left[1-\frac{p^2}{4b^2}\left(1-\frac{\tau}{r}\right)\right] = b^2\left\{\frac{\hat{\varphi}}{m_0\mathrm{Gi}^{\beta}}\right\}^2 Y^{(1-2\beta)/\Delta_1}, \quad (7)$$

where $\hat{\varphi} = \varphi[1 + v_1 \exp(-10\varphi)] + d_1\tau$, the coefficients m_0, v_1, d_1 and Gi are the system-dependent parameters, while the universal parameters p^2 and b^2 can be set equal to the linear model (LM) parameter $p^2 = b^2 = b^2_{\mathrm{LM}} = 1.359$ [36]. The coefficient v_1, which is supposed to be positive and small ($0 \le v_1 \ll 1$), ensures that at the triple point a physically obvious condition $Y = 1$ is captured in the model. In order to avoid an unphysical divergence of the kernel term when $|\tau| > 1$, one also needs to replace the crossover asymptotic equation for $K(\tau, \varphi)$, Eq. (4), with a modified expression:

$$K(\tau,\varphi) = \frac{\tau^2}{2(1+\tau^2)}\{a_{20}[Y^{-\alpha/\Delta_1}(\tau,\varphi)-1] + a_{21}[Y^{-(\alpha-\Delta_1)/\Delta_1}(\tau,\varphi)-1]\}. \quad (8)$$

This expression provides a better convergence to the classical behavior $Y \to 1$ and $K \to 0$ when $|\tau| \gg 1$ [38]. We need to note, that with these modifications, the crossover formulation of the Helmholtz free energy in the GC/CRS model is similar to the crossover EoS model for square-well fluids developed earlier [38].

Eq. (7) is a transcendental equation with respect to r and can be only solved numerically, making the calculation of the crossover function Y and its first and second derivatives more complicated. In practice, however, one can determine the parametric variable $r(\tau, \varphi)$ from the analytical sine (ANS) model developed recently by Kiselev and Ely [41]. Therefore, in the second step, we have also modified the GC/ANS model by using the parametric variable given r by [41]

$$r = \frac{2}{3}\left\{\left(\frac{b}{m_0}|\hat{\varphi}|\right)^{1/\beta} + \frac{1}{2}\tau + \sqrt{\left[\left(\frac{b}{m_0}|\hat{\varphi}|\right)^{1/\beta} + \frac{1}{2\tau}\right]^2 + \frac{3}{4}\tau^2}\right\}. \quad (9)$$

As we have shown earlier [41], in the asymptotic critical region, where $r \to 0$, both models, the GC/CRS given by Eqs. (1)–(3), (7) and (8), and the GC/ANS given by Eqs. (1)–(3) and (8) and (9), are physically equivalent. The main difference is that the derivatives $(\partial Y/\partial\tau)_\eta$, $(\partial Y/\partial\varphi)_\tau$, $(\partial^2 Y/\partial\tau^2)_\eta$, $(\partial^2 Y/\partial\varphi^2)_\tau$, and $(\partial^2 Y/\partial\tau\partial\varphi)$ in the GC/ANS model can be evaluated analytically and, therefore, the GC/ANS model is easier to use in practical applications.

Similar to the GC EoS [28], in the GC/CRS and GC/ANS models we use the Patel–Teja (PT) EoS [42,43] as a reference cubic EoS for one-component fluids. The "global" equation of state can be obtained by differentiation of Eq. (1) with respect to volume:

$$P(v,T) = -RT\left(\frac{\partial\bar{A}}{\partial v}\right) = \frac{RT}{v_{0c}} \times \left\{-\frac{v_{0c}}{v_c}\left[\left(\frac{\partial\Delta\bar{A}}{\partial\varphi}\right)_T - \left(\frac{\partial K}{\partial\varphi}\right)_\tau\right] + \bar{P}_0(T)\right\}, \quad (10)$$

where the dimensionless Helmholtz free energy $\bar{A}$ is determined by Eqs. (1)–(3), with using the replacements $\Upsilon \to Y$, and Eq. (8) for the kernel term.

Table 1
System-dependent constants for the GC/CRS model, Eqs. (1)–(3), (7) and (8)

	CH_4	C_2H_6	CO_2	H_2O
Classical critical parameters				
Z_{0c}	3.333329×10^{-1}	3.258977×10^{-1}	3.185531×10^{-1}	2.744415×10^{-1}
T_{0c} (K)	1.905640×10^{2}	3.053220×10^{2}	3.041282×10^{2}	6.47096×10^{2}
ρ_{0c} (mol l^{-1})	8.708162	5.887651	9.158456	1.494270×10^{1}
Critical shift				
Δv_c	-1.396796×10^{-1}	-1.417594×10^{-1}	-1.380162×10^{-1}	-1.660035×10^{-1}
c_1	-2.276827×10^{-1}	1.737651	2.097987×10^{1}	6.604890×10^{-1}
c_2	−1.844858	-1.621735×10^{-2}	2.561467×10^{1}	2.866304
c_3	8.515276×10^{-1}	−2.909159	-4.321730×10^{1}	−9.247295
Crossover parameters				
Gi	8.875467×10^{-2}	1.530256×10^{-1}	1.169050×10^{-1}	1.589771×10^{-1}
m_0	1.316678	1.287753	1.336174	1.395591
v_1	2.524273×10^{-3}	5.568065×10^{-3}	4.484512×10^{-3}	2.114637×10^{-3}
d_1	8.351856×10^{-1}	-3.497820×10^{-1}	1.276830	2.855061
a_{20}	4.392332	1.631400×10^{1}	7.220079	4.377004
a_{21}	−2.836717	2.699469	−3.574001	−7.72628

Table 2
System-dependent constants for the GC/ANS model, Eqs. (1)–(3), (8) and (9)

	CH_4	C_2H_6	CO_2	H_2O
Classical critical parameters				
Z_{0c}	3.321264×10^{-1}	3.243231×10^{-1}	3.137072×10^{-1}	2.663585×10^{-1}
T_{0c} (K)	1.905640×10^{2}	3.053220×10^{2}	3.041282×10^{2}	6.470960×10^{2}
ρ_{0c} (mol l^{-1})	8.739797	5.916235	9.299927	1.539616×10^{1}
Critical shift				
Δv_c	-1.270853×10^{-1}	-1.375926×10^{-1}	-1.247012×10^{-1}	-1.406946×10^{-1}
Classical PT EoS parameters				
c_1	-2.462321×10^{-1}	1.263169	4.065855×10^{1}	4.730452
c_2	−1.897490	-6.819121×10^{-1}	4.985292×10^{1}	2.170701
c_3	9.060517×10^{-1}	−1.889157	-8.294750×10^{1}	−8.084029
Crossover parameters				
Gi	7.941293×10^{-2}	1.330732×10^{-1}	8.593281×10^{-2}	8.405396×10^{-2}
m_0	1.625190	1.519874	1.717345	1.957081
v_1	1.134638×10^{-3}	3.042934×10^{-3}	3.331977×10^{-3}	1.728209×10^{-3}
d_1	6.978983×10^{-1}	-4.056100×10^{-1}	9.357659×10^{-1}	3.216950
a_{20}	4.844775	1.631400×10^{1}	6.951048	3.709276
a_{21}	−2.711996	2.701719	−2.289222	−9.282964

3. Comparison with experimental data

3.1. Thermodynamic properties

In general, the GC/CRS and GC/ANS models defined above are similar to the GC EoS for one-component fluids developed earlier [28] in that they require six classical system-dependent parameters and seven crossover parameters. Those parameters are the critical parameters T_{0c}, v_{0c}, Z_{0c}, and coefficients c_i ($i = 1$–3) in the $\alpha_a(T)$-term in the PT EoS, the Ginzburg number Gi, the critical shift Δv_c, the coefficients m_0, v_1, d_1, and the kernel term amplitudes a_{20} and a_{21}. Thus, the global crossover Helmholtz free energy for the GC/CRS and GC/ANS models contains 13 adjustable parameters. However, since the real critical parameters T_c, P_c, and Z_c for a one-component fluid are usually known, the critical shift $\Delta v_c = v_c/v_{0c} - 1$ is known too. Therefore, following our previous work [28], we use here the conditions $T_{0c} = T_c$ and $P_{0c} = P_c$ thus reducing the number of adjustable parameters to ten: the classical compressibility factor Z_{0c}, the coefficients c_i ($i = 1$–3), the Ginzburg number Gi, the coefficients m_0, v_1, d_1, and the critical amplitudes a_{20} and a_{21}.

In this work, we tested the GC/CRS and GC/ANS models against experimental data for methane, ethane, carbon dioxide, and water. For optimization of these models, we used the same data sets and optimization procedure as for the GC EoS [28]. In particular, the classical compressibility factor Z_{0c}, the Ginzburg number Gi, and the coefficients c_i ($i = 1$–3), m_0, v_1, and

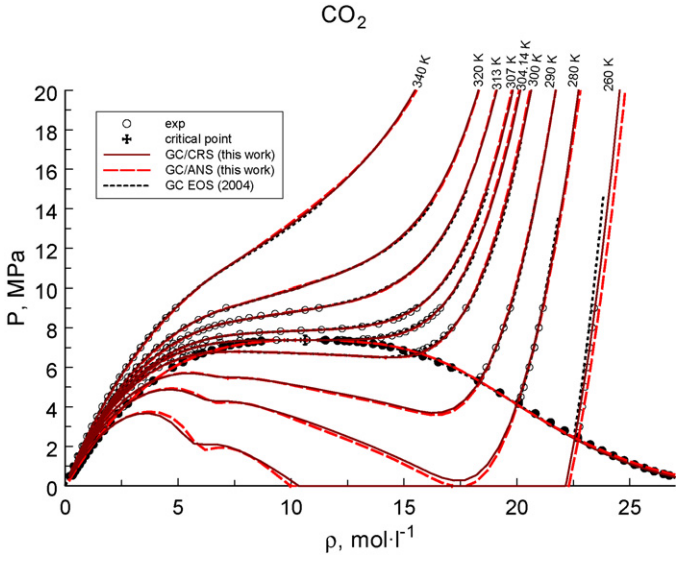

Fig. 2. $P\rho T$ data for carbon dioxide [48,49] compared to predictions of the GC/CRS model (solid curves), the GC/ANS model (long-dashed curves), and the GC EoS [28] (short-dashed curves). The empty symbols correspond to the one-phase region, and the filled symbols indicate the VLE data.

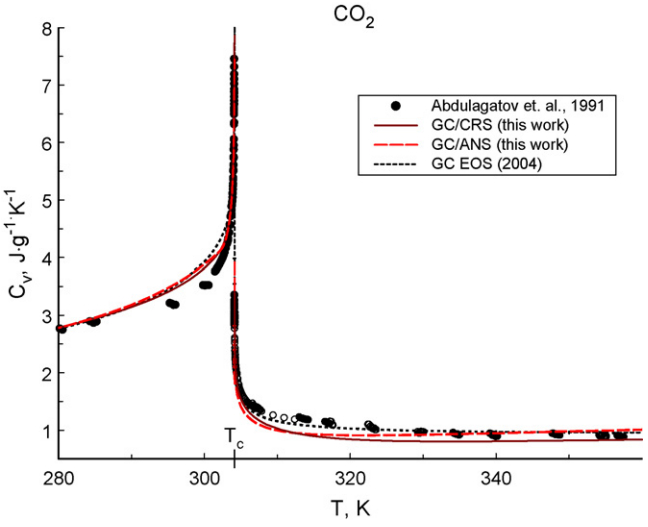

Fig. 3. The isochoric heat capacity data along the critical isochore [50] for carbon dioxide compared to predictions of the GC EoS [28] (short-dashed curves), the GC/CRS (solid curves), and the GC/ANS (long-dashed curves) models.

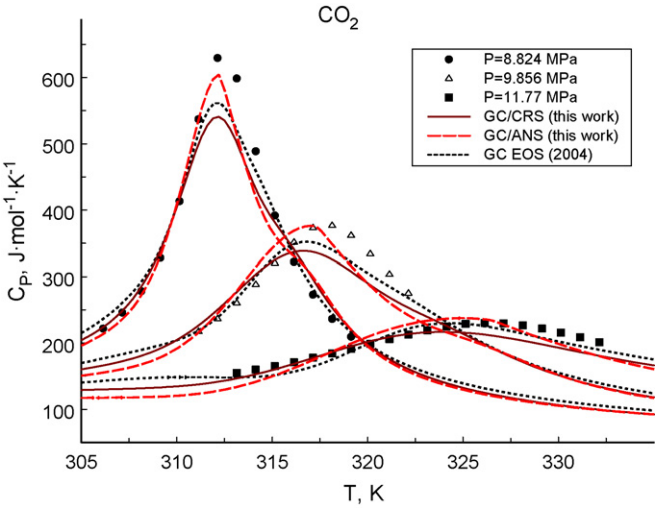

Fig. 4. The isobaric heat capacity data [51] for carbon dioxide compared to predictions of the GC EoS [28] (short-dashed curves), the GC/CRS (solid curves), and the GC/ANS (long-dashed curves) models.

d_1 were found from a fit of the models to experimental VLE- and PVT-data in one and two-phase regions. The amplitudes a_{20} and a_{21} for all substances were found from a fit of the models to the C_V-data generated along the critical isochore using the parametric crossover model developed for these substances by Kiselev and co-workers [44,45]. The system-dependent parameters for methane, ethane, carbon dioxide and water are listed for the GC/CRS and GC/ANS models in Tables 1 and 2, respectively. Comparisons of the predictions of the models with experimental data, and the GC EoS [28] as well, are shown in Figs. 2–6.

In Fig. 2 we show a comparison of the GC/CRS, GC/ANS, and GC EoS predictions with experimental PVT and VLE data for carbon dioxide. As one can see, in a wide range of thermodynamic states, all three models practically coincide and yield very good representation of the PVT and VLE surfaces of the pure fluids including the critical region. Similar to the GC EoS [28], the GC/CRS and GC/ANS models reproduce the PVT surface in the one-phase with an average absolute deviation (AAD) for pressure is less then 1%, and at $\rho \geq 2\rho_c$ they reproduce the liquid densities for all substances with an AAD of about 1–2%. We should note, that contrary to the GC EoS, the GC/CRS and GC/ANS models can be also extrapolated into the high temperature region (see solid and long-dashed curves in Fig. 1) without producing the non-monotonic unphysical behavior of the pressure-density isotherms discussed above for the GC EoS. The predictions of the GC/CRS and GC/ANS models for the PVT and VLE surface in methane, ethane, and water are also very similar to the ones achieved with the GC EoS [28], and, therefore, we will not show them here. For all substances in the temperature region $0.3T_c \leq T \leq T_c$, the GC EoS reproduces the saturated pressure data with an AAD of about 0.5–1%, the liquid density data with an AAD of about 1–2%, and the vapor density with about 2–3%.

Predictions for the one and two-phase isochoric heat capacity of carbon dioxide are shown in Fig. 3. The GC EoS results are shown as short-dashed curves and the GC/CRS are shown as solid curves. As one can see, in the asymptotic critical region the predictions of the GC EoS qualitatively and quantitatively are in a good agreement with experimental data. Similar results have been obtained for all other substances.

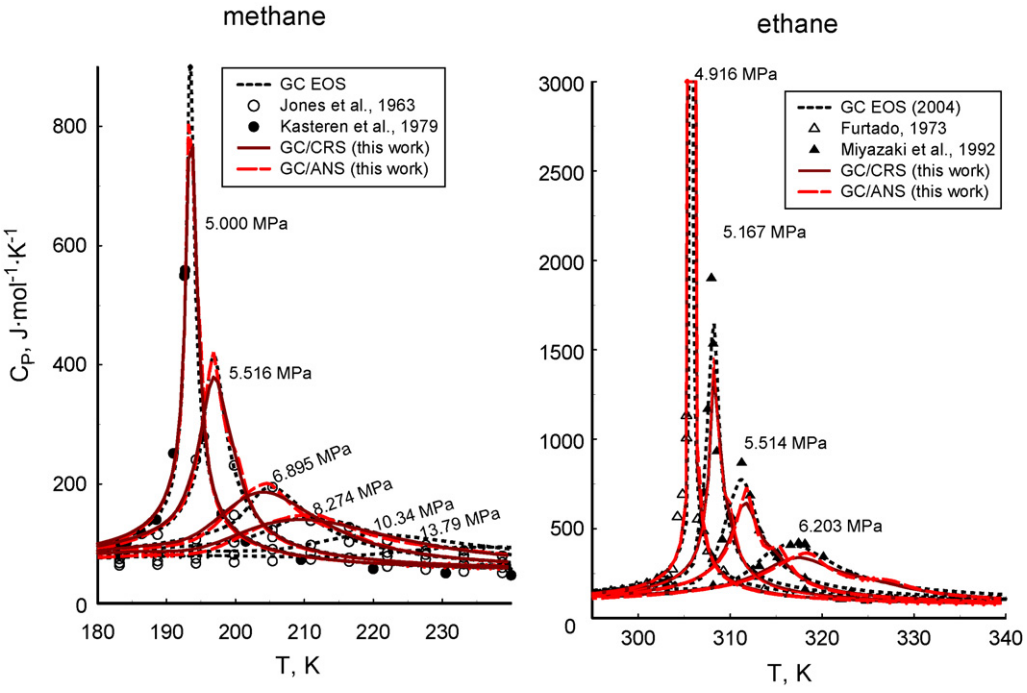

Fig. 5. The isobaric heat capacity data for methane [52,53] (left) and ethane [54,55] (right) compared to predictions of the GC EoS [28] (short-dashed curves), the GC/CRS (solid curves), and the GC/ANS (long-dashed curves) models.

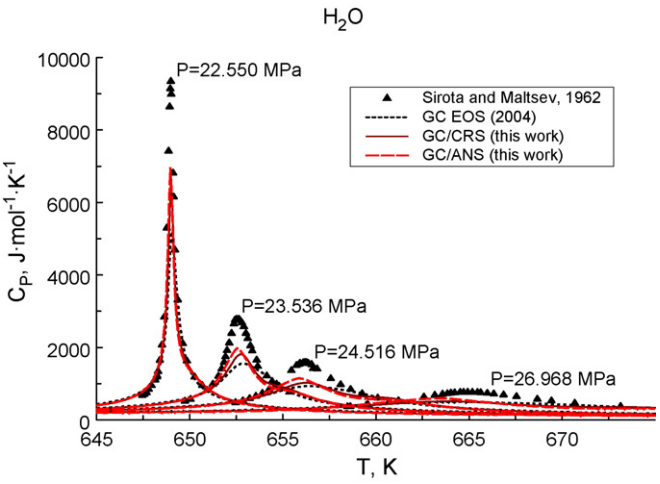

Fig. 6. The isobaric heat capacity data for water [56] compared to predictions of the GC EoS [28] (short-dashed curves), the GC/CRS (solid curves), and the GC/ANS (long-dashed curves) models.

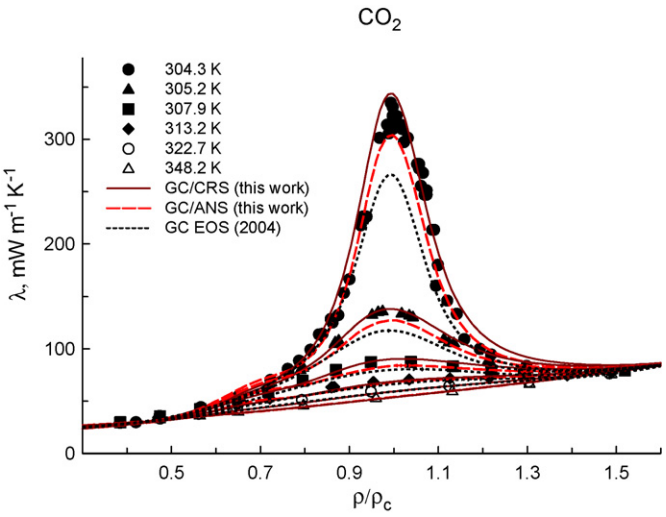

Fig. 7. The thermal conductivity data along the isotherms for carbon dioxide [57] compared to predictions of the GC + DMT [28] (short-dashed curves), the GC/CRS + DMT (solid curves), and the GC/ANS + DMT (long-dashed curves) models.

In Figs. 4–6 we compare experimental values of the isobaric heat capacities, C_p, with the values calculated with the GC/CRS and GC/ANS models (solid and long-dashed curves, respectively), and the GC EoS (short-dashed curves). Again, all three models give the very similar predictions, which in the critical region are systematically lower than experimental values. As we noted in it our previous work [28], this is not surprising, since a simple cubic EoS, even in the crossover formulation, is unable to simultaneously reproduce the PVT and heat capacity data in the critical region within experimental accuracy. Except for data points very close to the critical point, for which deviations increase to 30–40%, the GC EoS reproduces the isobaric heat capacity data shown in Figs. 3 and 4 with an AAD of about 2–5% in the low-density region, and with an AAD of about 1–2% for liquids. Thus, in spite of the differences in definition of the crossover function, the GC/CRS and GC/ANS models give a sufficiently accurate representation of the isochoric and isobaric heat capacities in pure fluids and, therefore, can be used for the prediction the thermal conductivity in the critical region.

3.2. Thermal conductivity

Following our previous work [28], we use a crossover decoupled-mode theory (DMT) expression for the calculation

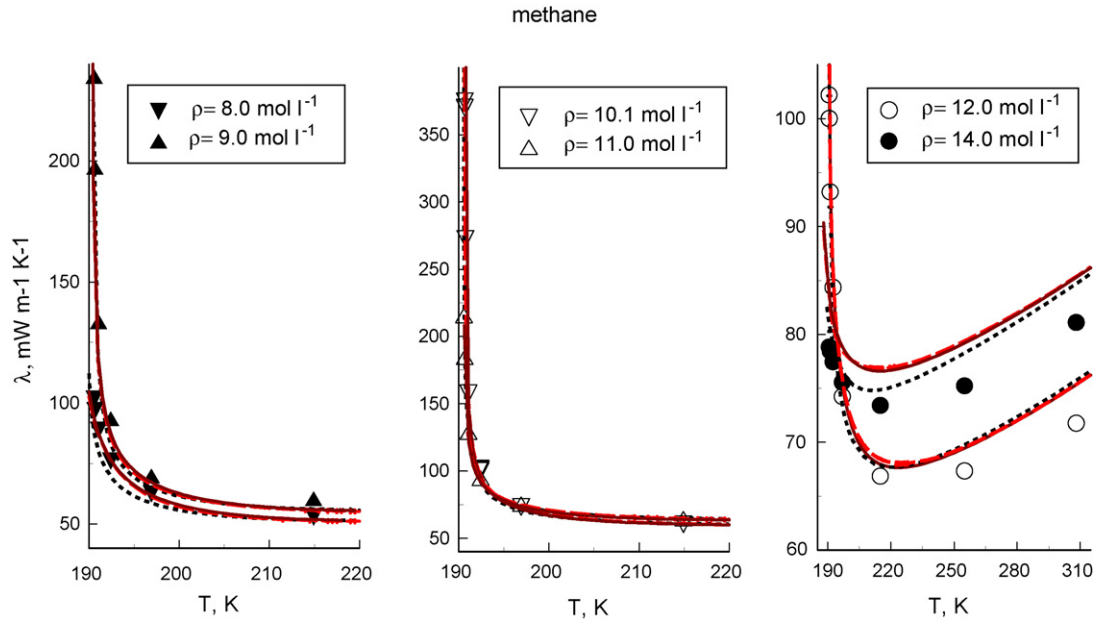

Fig. 8. The thermal conductivity data along the isochores for methane [58] (symbols) compared to predictions of the GC + DMT [28] (short-dashed curves), the GC/CRS + DMT (solid curves), and the GC/ANS + DMT (long-dashed curves) models.

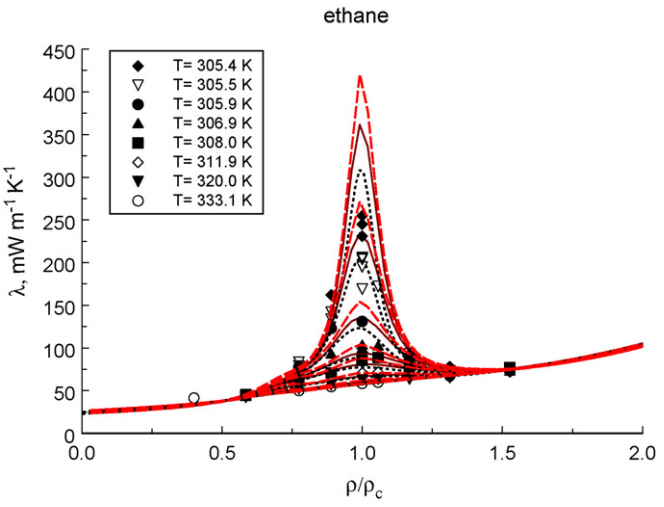

Fig. 9. The thermal conductivity data along the isotherms for ethane [59] (symbols) compared to predictions of the GC + DMT [28] (short-dashed curves), the GC/CRS + DMT (solid curves), and the GC/ANS + DMT (long-dashed curves) models.

of the thermal conductivity in the critical region [46,47]:

$$\lambda = \frac{k_B T \rho C_p}{6\pi\eta\hat{\xi}}\Omega(z) + \lambda_b. \quad (11)$$

In this equation, k_B is Boltzmann's constant, η the shear viscosity, and λ_b is a background part of the thermal conductivity which is an analytic function of the temperature and density. For the crossover function $\Omega(z) = \Omega(q_D\hat{\xi})$ and renormalized correlation length $\hat{\xi}(T, \rho)$ we use the same expressions and the same system-dependent parameters ξ_0 and q_D as employed in our previous work [28] (see Eqs. (13)–(16) in Ref. [28]). Here, however, the thermodynamic properties were calculated with the GC/CRS and GC/ANS models developed in this work. For the shear viscosity $\eta(T, \rho)$ and background part of the thermal conductivity $\lambda_b(T, \rho)$ we also use the same correlations as in our previous GC + DMT model [28] (see Eqs. (20) and (21) in Ref. [28]).

A comparison of thermal conductivity data for carbon dioxide, methane, and ethane with the predictions of the GC + DMT, GC/CRS + DMT, and GC/ANS + DMT models is shown in Figs. 7–9.

In agreement with experimental data, all models yield an anomalous increase in the thermal conductivity in the critical region, while far away from the critical point they reduce to their background contributions. Also when $\rho \to 0$, all models give the dilute gas contribution $\lambda_0(T)$. Since the DMT expression for the thermal conductivity, Eq. (11), involves not only direct P–ρ–T calculations but also require an accurate representation of the first, $(\partial P/\partial\rho)_T$ and $(\partial P/\partial T)_\rho$, and second, $(\partial^2 P/\partial T^2)_\rho$, derivatives, we consider the results presented in Figs. 7–9 as additional proof of the thermodynamic self consistency of the GC/CRS and GC/ANS models developed in this work.

List of symbols

a_{2i}	parameter in Eq. (4) ($i = 0,1$)
A	Helmholtz free energy
$\bar{A}$	dimensionless Helmholtz free energy
$\bar{A}_0$	dimensionless ideal gas part of free energy
$\bar{A}_0^{res}$	dimensionless ideal residual part along the critical isochore
b^2	universal linear-model parameter
c_i	system-dependent parameters in the Patel–Teja EoS ($i = 1$–3)
C_P	isobaric heat capacity
C_V	isochoric heat capacity
d_1	system-dependent coefficient
g	inverse Ginzburg number
Gi	Ginzburg number
k_B	Boltzmann's constant
m_0	system-dependent coefficients
M_w	molecular weight
p^2	universal sine-model parameter
P	pressure
P_c	critical pressure
$\bar{P}_0$	dimensionless pressure along the critical isochore
q, $\hat{q}$	arguments of the crossover functions
q_D	cut-off wave number
R	gas constant
T	temperature (K)
T_c	critical temperature (K)
v	molar volume ($l\,mol^{-1}$)
v_c	critical volume ($l\,mol^{-1}$)
v_1	system-dependent coefficient
z	argument of the dynamical crossover function
Z_c	critical compressibility factor
Υ, Y	crossover functions

Greek letters

α	universal critical exponent
β	universal critical exponent
Δ	difference
Δ_1	universal critical exponents
γ	universal critical exponent
η	shear viscosity
φ	order parameter
$\bar{\varphi}$	renormalized order parameter
K	kernel term
λ	thermal conductivity
ρ	molar density ($mol\,l^{-1}$)
τ	reduced temperature difference
$\bar{\tau}$	renormalized temperature difference
ξ	correlation length
ξ_0	critical amplitude

Subscripts

bg, b	background
c	critical
ex	excess
0	classical

Superscripts

id	ideal gas part
res	residual

Acknowledgment

The authors are indebted to Prof. Sergio E. Quiñones-Cisneros from the University of Colonge, Koeln, Germany for calling our attention to this problem.

References

[1] J.R. Fox, Method for construction of nonclassical equations of state, Fluid Phase Equilib. 14 (1983) 45–53.
[2] J.R. Fox, T.S. Strovick, A field-space conformal solution method: binary vapor–liquid phase behavior, Int. J. Thermophys. 11 (1) (1990) 61–72.
[3] A. Parola, L. Reatto, Liquid-state theory for critical phenomena, Phys. Rev. Lett. 53 (25) (1984) 2417–2420.
[4] A. Parola, L. Reatto, Hierarchical reference theory of fluids and the critical point, Phys. Rev. A 31 (5) (1985) 3309–3322.
[5] A. Parola, A. Meroni, L. Reatto, Theory of the universal and nonuniversal quantities of fluids at the critical point, Int. J. Thermophys. 10 (2) (1989) 345–356.
[6] M. Tau, et al., Differential theory of fluids below the critical temperature: study of Lennard–Jones fluid and of a model C60, Phys. Rev. E 52 (1995) 2644–2655.
[7] L. Reatto, A. Parola, Liquid-state theory and the renormalization group reconciled: theory of phase transitions in fluids, J. Phys. Condens. Matter 8 (1996) 9221–9231.
[8] D. Pini, A. Parola, L. Reatto, A comprehensive approach to critical phenomena and phase transitions in binary mixtures, Int. J. Thermophys. 19 (6) (1998) p1545.
[9] D. Pini, G. Stell, N.B. Wilding, A liquid-state theory that remains successful in the critical region, Mol. Phys. 95 (1998) p483.
[10] P.C. Albright, et al., A crossover description for the thermodynamic properties of fluids in the critical region, Int. J. Thermophys. 7 (1) (1986) 75–85.
[11] A. Kostrowichka Wyszalkovska, M.A. Anisimov, J.V. Sengers, Global crossover equation of state of van der Waals fluid, Fluid Phase Equilib. 158–160 (1999) 523–535.
[12] A. van Pelt, G.X. Jin, J.V. Sengers, Critical scaling laws and classical equation of state, Int. J. Thermophys. 15 (4) (1994) 687–697.
[13] D.D. Erikson, T.W. Leland, Application of critical-region scaling to pure-component equation of state, Int. J. Thermophys. 7 (1986) 911.
[14] J.J. De Pablo, J.M. Prausnitz, Thermodynamics of liquid–liquid equilibria including the critical region. Transformation to non-classical coordinates using revised scaling, Fluid Phase Equilib. 59 (1) (1990) 1.
[15] J.A. White, S. Zhang, Renormalization theory of nonuniversal thermal properties of fluids, J. Chem. Phys. 103 (5) (1990) 1922.
[16] J.A. White, S. Zhang, Renormalization group theory for fluids, J. Chem. Phys. 99 (3) (1993) 2012.
[17] J.A. White, Lennard–Jones as a model for argon and test of extended renormalization group calculations, J. Chem. Phys. 111 (20) (1999) 9352.
[18] J.A. White, Global renormalization calculations compared with simulations for Lennard–Jones fluid, J. Chem. Phys. 112 (7) (2000) 3236.
[19] J.A. White, Are global renormalization methods capable of locating gas–liquid critical points? Int. J. Thermophys. 22 (4) (2001) 1147–1157.
[20] T. Kraska, U.K. Deiters, An equation of state for pure fluids describing the critical region, Int. J. Thermophys. 15 (2) (1994) 261–281.
[21] T. Kraska, An equation of state describing the critical region: extension to high pressure, J. Supercrit. Fluids 16 (1) (1999) 1.
[22] Y. Tang, Outside and inside the critical region of the Lennard–Jones fluid, J. Chem. Phys. 109 (14) (1998) 5935–5944.
[23] L. Lue, J.M. Praustitz, Renormalization-group corrections to an approximate free-energy model for simple fluids near to and far from the critical point, J. Chem. Phys. 108 (13) (1998) 5529–5536.
[24] L. Lue, J.M. Praustitz, Thermodynamics of fluid mixtures near to and far from the critical region, AIChE J. 44 (6) (1998) 1455–1466.
[25] F. Fornasiero, L. Lue, A. Bertucco, Improving cubic EoSs near the critical point by a phase-space cell approximation, AIChE J. 45 (4) (1999) 906–915.
[26] J. Jiang, J.M. Prausnitz, Equation of state for thermodynamic properties of chain fluids near-to and far-from the vapor–liquid critical region, J. Chem. Phys. 111 (13) (1999) 5964.
[27] J. Jiang, J.M. Prausnitz, Critical temperatures and pressures for hydrocarbon mixtures from an equation of state with renormalization-group theory corrections, Fluid Phase Equilib. 169 (2000) 127–147.
[28] S.B. Kiselev, J.F. Ely, Generalized crossover description of the thermodynamic and transport properties in pure fluids, Fluid Phase Equilib. 222–223 (2004) 149–159.
[29] L. Sun, S.B. Kiselev, J.F. Ely, Multiparameter crossover equation of state: generalized algorithm and application to carbon dioxide, Fluid Phase Equilib. 233 (2005) 270–285.
[30] J.V. Sengers, J.M.H. Levelt Sengers, Thermodynamic behavior of fluids near the critical point, Annu. Rev. Phys. Chem. 37 (1986) 189–222.
[31] M.A. Anisimov, S.B. Kiselev, Universal crossover approach to description of thermodynamic properties of fluids and fluid mixtures, in: A.E. Scheindlin, V.E. Fortov (Eds.), Sov. Tech. Rev. B: Therm. Phys., Part 2, Harwood Academic, New York, 1992, pp. 1–121.
[32] S.B. Kiselev, Cubic crossover equation of state, Fluid Phase Equilib. 147 (1–2) (1998) 7–23.
[33] S.B. Kiselev, J.F. Ely, Crossover SAFT equation of state: application for normal alkanes, Ind. Eng. Chem. Res. 38 (12) (1999) 4993–5004.
[34] S.B. Kiselev, D.G. Friend, Cubic crossover equation of state for mixtures, Fluid Phase Equilib. 162 (1–2) (1999) 51–82.
[35] S.B. Kiselev, J.F. Ely, Generalized corresponding states model for bulk and interfacial properties of pure fluids and fluid mixtures, J. Chem. Phys. 119 (16) (2003) 8645–8662.
[36] S.B. Kiselev, J.F. Ely, Simplified crossover SAFT equation of state, Fluid Phase Equilib. 174 (2000) 93–119.
[37] M.Y. Belyakov, S.B. Kiselev, J.C. Rainwater, Crossover Leung–Griffiths model and the phase behavior of dilute aqueous ionic solutions, J. Chem. Phys. 107 (8) (1997) 3085–3097.
[38] S.B. Kiselev, et al., Computer simulations and crossover equation of state of square-well fluids, Fluid Phase Equilib. 200 (2002) 121–145.
[39] S.B. Kiselev, Universal crossover functions for the free energies of single-component and two-component fluids in their critical regions, High Temp. 28 (1) (1990) 42–49.
[40] S.B. Kiselev, I.G. Kostyukova, A.A. Povodyrev, Universal crossover behavior of fluids and fluid mixtures in the critical region, Int. J. Thermophys. 12 (5) (1991) 877–895.
[41] S.B. Kiselev, J.F. Ely, A new analytical formulation for the generalized corresponding states model for thermodynamic and surface properties in pure fluids, Chem. Eng. Sci. 61 (2006) 5107–5113.
[42] N.C. Patel, A.S. Teja, A new cubic equation of state for fluids and fluid mixtures, Chem. Eng. Sci. 37 (3) (1982) 463–473.
[43] N.C. Patel, Improvement of the Patel–Teja equation of state, Int. J. Thermophys. 17 (1996) 673–680.
[44] S.B. Kiselev, Prediction of the thermodynamic properties and the phase behavior of binary mixtures in the extended critical region, Fluid Phase Equilib. 128 (1–2) (1997) 1–28.
[45] S.B. Kiselev, D.G. Friend, Revision of a multiparameter equation of state to improve the representation in the critical region: application to water, Fluid Phase Equilib. 155 (1) (1999) 33–55.
[46] S.B. Kiselev, M.L. Huber, Transport properties of carbon dioxide + ethane and methane + ethane mixtures in the extended critical region, Fluid Phase Equilib. 142 (1998) 253–280.
[47] S.B. Kiselev, R.A. Perkins, M.L. Huber, Transport properties of refrigerants R32, R125, R134a, and R125 + R32 mixtures in and beyond the critical region, Int. J. Refrig. 22 (1999) 509–520.
[48] W. Duschek, R. Kleinrahm, W. Wagner, J. Thermodyn. Chem. 22 (1990) 827–841.
[49] R. Gilgen, R. Kleinrahm, W. Wagner, Supplementary measurement of the (pressure, density, temperature) relation of carbon dioxide in the region at temperatures range from 220 K to 360 K at pressures up to 13 MPa, J. Chem. Thermodyn. 24 (1992) 1243–1250.
[50] I.M. Abdulagatov, N.G. Polikhronidi, R.G. Batyrova, J. Chem. Thermodyn. 26 (1994) 1031–1045.
[51] S.L. Rivkin, V.M. Gukov, Teploenergetika (Russian) 18 (10) (1971) 82.

[52] M.L. Jones, et al., Chem. Eng. Prog. Symp. Ser. 59 (1963) 52.
[53] P.H.G. van Kasteren, Ind. Eng. Chem. Fundam. 18 (1979) 333.
[54] A. Furtado, Department of Chemical Engineering, University of Michigan, Ann Arbor, MI, 1973.
[55] T. Miyazaki, A.V. Hejmadi, J.E. Powers, J. Chem. Thermodyn. 12 (1980) 105.
[56] A.M. Sirota, B.K. Maltsev, Teploenergetika 1 (1962) 52.
[57] A. Michels, J.V. Sengers, P.S. van der Gulik, Physica 28 (1962) 1216.
[58] E.P. Sakonidou, Thermal Conductivity of Fluids and Fluid Mixtures in the Critical Region, University of Amsterdam, Amsterdam, 1990, p. 180.
[59] R. Mostert, The Thermal Conductivity of Ethane and its Mixtures with Carbon Dioxide in the Critical Region, University of Amsterdam, Amsterdam, 1992.